PET and SPECT Scanners

6

What we observe as material bodies and forces are nothing but shapes and variations in the structure of space. Particles are just schaumkommen (appearances). The world is given to me only once, not one existing and one perceived. Subject as well as object is only one. The barrier between them cannot be said to have broken down as a result of recent experience in the physical sciences, for this barrier does not exist.

Erwin Schrodinger

6.1 Interaction of Radiation with Matter

Radiation emitted by radionuclides can be classified into electromagnetic (such as x-rays, γ-rays, annihilation photons) or particulate (such as β^-, β^+) radiation. When we speak of the interaction of radiation with matter, we mean its interaction with the electrons and nucleus of atoms. The interaction of radiation, in general, may be classified as *elastic* or *inelastic*. In an elastic interaction, the incident radiation is scattered in a different direction, but the total energy of the interacting particles is conserved. In contrast, in an inelastic interaction, a certain amount of energy is lost.

Ionization occurs when an electron is ejected from an atom, producing an ion pair, a free electron, and a positive atom. High-energy photons (X-rays, γ-rays, and annihilation photons) and charged particles (β^-, β^+, H^+, and α or He^{2+}) are regarded as ionizing radiation. If an electron is not ejected from the atom but merely raised to higher energy levels or outer shells, the process is termed *excitation*, and the atom is said to be *excited*. In certain materials, when the electrons in the excited state drop to a lower energy state, with the emission of visible light, then that material is said to exhibit *luminescence*. If the production of light ceases within 10^{-8} s of the end of irradiation (or interaction), then the process is one of *fluorescence*; if it continues beyond this point, then the process is called *phosphorescence* (also known as *afterglow*).

6.1.1 Interactions of Charged Articles

6.1.1.1 Ionization

Charged particles (such as electrons β^-, β^+, and H^+) passing an absorbing medium transfer some of the energy to electrons of the medium and are then deflected. Therefore, they cause *ionization* and/or *excitation*. The probability of scattering increases with the atomic number Z of the absorbing medium, and decreases rapidly with the increasing kinetic energy of the incident electron. In a close encounter, an orbital electron may be separated from the atom, thus causing ionization. The ejected electron may have sufficient energy to cause secondary ionization and eject an orbital electron, known as delta (δ) rays. The *specific ionization* (SI), the number of primary and secondary ion pairs produced per centimeter in air, at standard temperature and pressure (STP), can be estimated on the basis of the velocity (v) of incident electron and the velocity of light (c) using the following equation:

$$\mathrm{SI} = \frac{45}{(v/c)^2} \tag{6.1}$$

A less close encounter of the incident charged particle with an atom or molecule may result in an orbital electron being raised to an excited state, thus causing atomic or molecular excitation. The energy absorbed by the atom is dissipated in the subsequent atomic emission of electromagnetic radiation (such as infrared, visible, or UV).

S. Vallabhajosula, *Molecular Imaging: Radiopharmaceuticals for PET and SPECT,*
DOI: 10.1007/978-3-540-76735-0_6, © Springer-Verlag Berlin Heidelberg 2009

6.1.1.2 Bremsstrahlung Radiation

When an incident β^- particle penetrates the electron cloud of an atom, it may interact with the nucleus and may be deflected with a reduced velocity. The energy lost by the incident electron will appear as electromagnetic radiation, known as bremsstrahlung (breaking radiation) (Fig. 6.1). The probability of bremsstrahlung varies with Z^2 of the absorbing medium.

6.1.1.3 Annihilation Radiation

A positron (β^+), after expending its kinetic energy in inelastic collisions, combines with an electron (β^-) of the absorbing medium. Both the particles are annihilated, and their mass appears as electromagnetic radiation (usually two 511-keV photons), known as annihilation radiation (Fig. 6.1). This interaction of β^- and β^+ particles (matter and antimatter) is called *pair annihilation*.

6.1.1.4 Cerenkov Radiation

Particles normally cannot exceed the velocity of light in a vacuum (3.0×10^{10} cm s^{-1}). Light, however, travels at slower speeds in different materials or media. It is possible for β^- rays to travel at speeds much higher than that of light in a specific medium. When this occurs, visible light, known as *Cerenkov radiation*, is emitted. For example, the blue glow seen near the core of a swimming pool reactor is due to Cerenkov radiation.

6.1.2 Interaction of High-Energy Photons

The interaction of electromagnetic radiation with atoms, electrons, and nuclei of different materials is generally regarded as a collision involving transfer of their energy to matter without necessarily causing ionization directly. However, certain interactions do eject orbital electrons, produce ion pairs, and cause ionization effects. Therefore high-energy photons, similar to charged particles, are regarded as ionizing radiation. However, unlike charged particles, high-energy photons being massless can penetrate soft-tissue thickness of >10 cm in vivo and are considered to be highly penetrating radiation.

The high-energy photons of x-rays, γ-rays, and annihilation radiation associated with radiotracers in nuclear medicine undergo inelastic interactions by means of several mechanisms. The *photoelectric effect* and *Compton scattering* are important in radiation detection and measurement. Pair production and photodisintegration have a high energy threshold (>1 MeV) and are not relevant to the photon energies normally encountered in nuclear medicine.

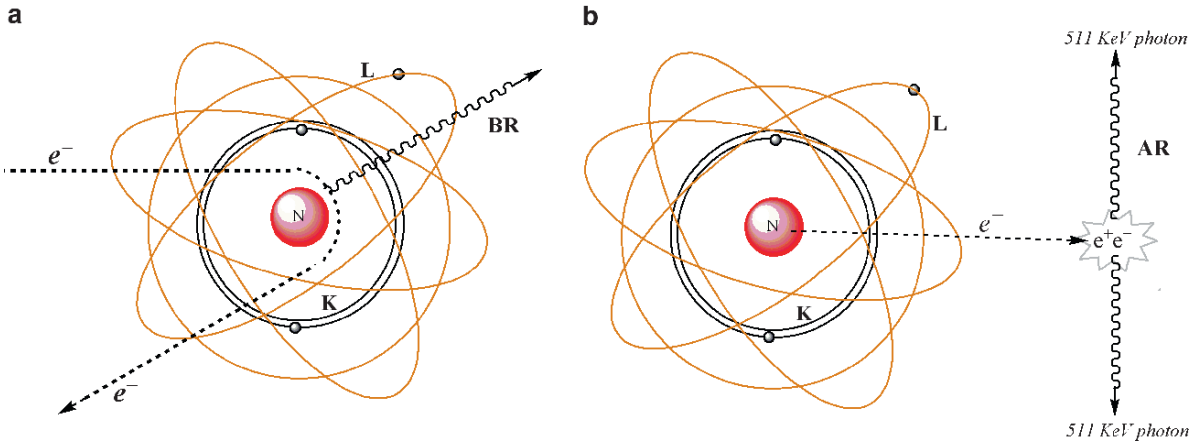

Fig. 6.1 Interaction of charged particles with matter. When high-energy electrons penetrate and approach the nucleus, they are decelerated and deflected (**a**). As a result, bremstrahlung radiation (BR) is produced. The positron emitted from the atomic nucleus finally interacts with an electron and annihilates it (**b**). As a result, annihilation radiation (AR) is produced in which two photons with a minimum of 511 keV energy travel in opposite directions

6.1.2.1 Photoelectric Effect

When a metal is exposed to electromagnetic radiation, electrons are ejected from the metal (Fig. 6.2). These electrons are called *photoelectrons*. Light with shorter wavelengths (such as UV) ejects electrons with greater speed. Thus the kinetic energy of photoelectrons is dependent on the frequency, however, the number of electrons ejected depends on the intensity of the electromagnetic radiation. Different metals have different threshold values for the frequency. Depending on the Z of the element, electrons may be held more loosely or tightly. Einstein was able to show that photons with higher energy eject electrons with greater kinetic energy. This phenomenon of the photoelectric effect is very important for the interaction of radiation with matter and for developing radiation detectors. The photoelectric effect should obey the following relationship:

$$h\nu = KE_{max} + \varphi \tag{6.2}$$

where

$$\varphi = h\nu_0 \tag{6.3}$$

Also, ν_0 is the critical frequency below which no photoelectric effect occurs and ϕ is the minimum energy (called the *work function* of the metal) needed for the electron to escape from a metal surface. The photoelectric effect is an atomic absorption process in which an atom totally absorbs the energy of the incident photon. It is an interaction of photons with orbital electrons in an atom, mostly the inner-shell electrons, in which the photon transfers all of its energy to the electron, which is then ejected. Some of the energy of the incident photon is used to overcome the binding energy of the electron, and the remaining energy is given to the photoelectron, as kinetic energy. Since the ejection of a photoelectron creates a vacancy in the inner shell, the photoelectric effect is usually accompanied by the emission of characteristic x-rays and/or Auger electrons.

The probability of a photoelectric interaction occurring at a particular shell depends on the energy of the incident photon and the binding energy of the shell (in other words, on Z). The probability is zero when the energy of photon is less than the binding energy of electron; it is greatest when the photon energy is equal to the binding energy of electron and thereafter decreases rapidly with increasing photon energy. Following the injection of radiotracers, the photoelectric effect plays a minor role with soft tissue. In radiation detectors, such as scintillation detectors, however, the photoelectric effect is the predominant mode of interaction of photons.

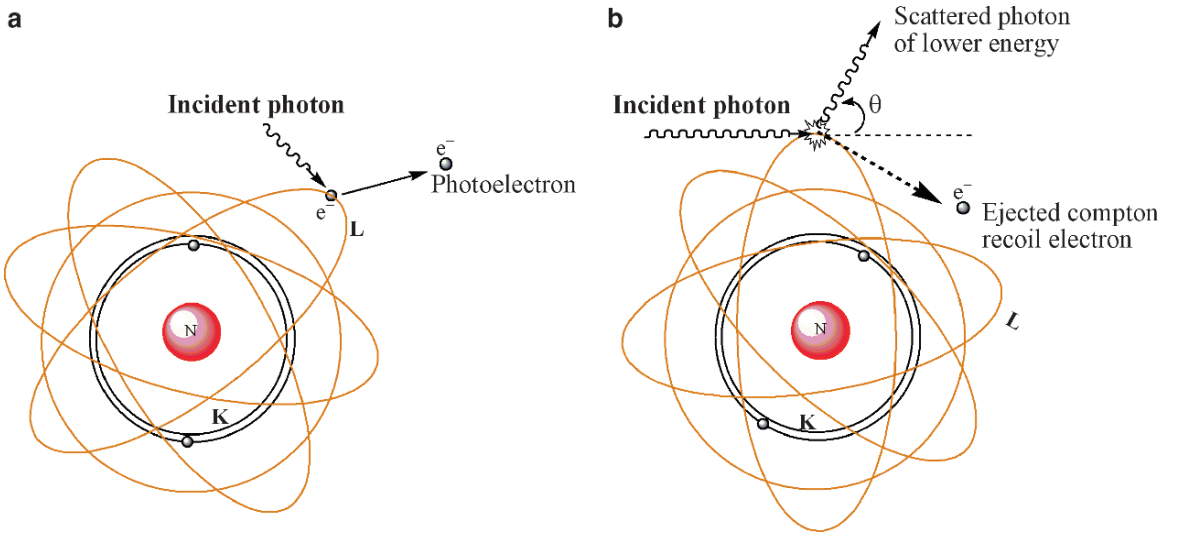

Fig. 6.2 Interaction of high-energy photons with matter. In the photoelectric effect (**a**), an incident photon transfers all its energy to an orbital electron, which leaves the atom and is known as a photoelectron. In Compton scattering (**b**), the incident photon transfers only part of its energy to an orbital electron, which is then ejected (recoil electron). The scattered photon is then deflected in a different angle (θ, the scattering angle)

6.1.2.2 Compton Scattering

Compton scattering is a collision between a photon and a loosely bound outer orbital electron. After the interaction, the *scattered photon* undergoes a change in direction and the recoil electron is ejected from the atom (Fig. 6.2). The scattered photon is deflected through an angle (θ_C) proportional to the amount of energy lost. The maximum energy loss occurs when the θ_C is 180° or when the photon is *backscattered*. For example, the annihilation photon (511 keV) after backscatter will have an energy of 170 keV. The energy lost by the scattered photon is divided between the small binding energy of the orbital electron and the kinetic energy of the recoil electron. The relative probability of Compton scattering increases slightly as the energy of the incident photon increases and as the effective atomic number (Z_{eff}) of the interacting medium decreases. Following administration of radiotracers, the most important and significant mode of interaction of photons with soft tissue is Compton scattering.

6.1.2.3 Pair Production

When a high-energy photon interacts with an electric field of a charged particle (atomic nucleus or even an electron), the incident photon may completely disappear and its energy is used to create a β^- and β^+ pair, known as *pair production*. Since the rest of the energy of the electron is 511 keV, the incident photon must have a minimum energy of 1.022 MeV. The difference between the incident photon energy and 1.022 MeV is imparted to the electron pair as kinetic energy.

6.1.3 Attenuation

If we measure the intensity of the radiation before (I_0) and after it interacts with a given medium (I_x) of particular thickness x, we find that the intensity of the radiation after passing through the medium has reduced; the beam of radiation is said to have been attenuated. By the processes of absorption and scattering in a medium, a beam of radiation undergoes attenuation. The atoms in the medium act as targets, which, if hit, will attenuate a photon from the primary radiation beam. The probability of an interaction with a particular atom is low, but the very large number of atoms in a small volume of a solid increases the probability of attenuation, significantly. A parallel beam of monoenergetic electromagnetic radiation will undergo exponential attenuation as it passes through a uniform medium.

$$I_x = I_0 e^{-\mu x} \tag{6.4}$$

where μ is the total *linear attenuation coefficient*, which can be defined as the fraction of photons removed from a beam of radiation per unit thickness of the attenuating medium. The parameter μ is a property of both the photon energy and the nature of the medium. It increases (i.e., photons become less penetrating) for low photon energies and low mass density. In a given thickness of medium, the number of atoms (N) may be the same for different materials, but the density (ρ) may vary. Therefore, the total mass attenuation coefficient μ/ρ is the fraction of photons removed from a beam of radiation of unit cross-sectional area by unit mass of the medium. For photons with <1 MeV energy, the parameters μ and μ/ρ are largely made up of components due to photoelectric absorption (τ) and Compton scattering (σ).

Other important parameters derived from μ are half-value thickness (HVT) or half-value layer (HVL), tenth value layer (TVL), and the mean free path (MFP), which is the distance a photon (or a particle) travels before interacting. All these parameters are related mathematically as shown in the following equations:

$$\mu = 0.693 / \text{HVL} \tag{6.5}$$

$$\text{MFP} = 1.44\ \text{HVL} \tag{6.6}$$

With radiation, the three most important media of interest are the tissue, radiation detector material (the crystal), and the type of shielding (lead, tungsten). For various materials, the linear attenuation coefficient and HVL values for photons of two different energies, 140 and 511 keV, are shown in Table 6.1. For 511-keV photons, the primary interaction is Compton scattering; therefore, correction for attenuation and scattering is essential for PET imaging studies.

Table 6.1 Linear attenuation coefficient and HVL values of photons for different materials

	Density (ρ)	140-keV photon		511-keV photon	
Material	(g cm^{-3})	μ (cm^{-1})	HVL	μ (cm^{-1})	HVL
Water	1.0	0.15	4.62	0.095	7.29
Adipose tissue	0.95	0.142	4.88	0.090	7.70
Cortical bone	1.92	0.284	2.44	0.178	3.89
Pyrex glass	2.23	0.307	2.26	0.194	3.57
Lucite	1.19	0.173	4.01	0.112	6.19
NaI (Tl)	3.67	2.23	0.31	0.34	2.04
Bismuth germinate	7.13	~5.5		0.95	0.73
Lead	11.35	40.8	0.018	1.75	0.42
Tungsten				2.59	0.29

6.2 Radiation Detectors

Radiation detectors have been developed over the years on the basis of the two major consequences of interaction of radiation with matter; ionization and excitation. Radiation detectors are generally categorized as either ionization detectors or scintillation detectors.

6.2.1 Ionization Detectors

These detectors respond to radiation by means of ionization, which induces tiny electrical currents that can be detected and measured. The ionization detectors can be either gas-filled (also known as *ionization chambers*) or *semiconductor detectors*.

6.2.1.1 Gas-filled Detectors

Most gas-filled detectors are made up of a chamber, which contains a volume of gas (mostly air or an inert gas) between two electrodes with a voltage difference between them. Under normal circumstances, the gas is an insulator and no current flows between the electrodes. When the gas is ionized following an interaction with radiation, electrons are attracted to the anode and positive ionized atoms are attracted to the cathode, producing a small current. When gas-filled chambers operate at the saturation voltage (300–600 V), to ensure complete collection of ions at the electrodes, they are called *ionization chambers*. If the detector is calibrated to express the measured current as an exposure rate (R h^{-1}, mR h^{-1}), it is called a survey meter; if it collects the total charge over a period of time, it is called a *pocket dosimeter*; and, finally, if the measured current is used to assay the activity (mCi, MBq, etc.), it is called a *dose calibrator*.

Ionization chambers are quite inefficient as detectors for X-rays and γ-rays. Their response to photons changes with photon energy, but the energy discrimination, especially in the case of dose calibrators, is achieved only by the use of precalibrated amplifiers, one for each radionuclide of interest.

If an ionization chamber is maintained between 900 and 1,200 V, the electrons generated by the interaction of radiation will accelerate and cause additional ionization. This process is known as *gas amplification* of the charge, and the factor by which the ionization is amplified is called the *gas amplification factor* (GAF). A Geiger–Muler (GM) counter is a gas-filled detector designed to have GAF as high as 10^{10}. In a GM counter, the size of the electrical signal output is relatively constant and independent of the energy of radiation. Because of their high sensitivity, GM counters are mainly used as survey meters to detect ambient radiation levels and radioactive contamination.

6.2.1.2 Semiconductor Detectors

Semiconductor detectors are essentially solid-state analogs of gas-filled detectors (Darambara and Todd-Pokropek 2002). Semiconductor materials, such as Si and Ge, when doped with Li, can function as solid ionization chambers, and are also called *solid-state detectors*. In order to create an ion pair in air, the energy needed is 34 eV per ionization. In contrast, the energy needed to create an ion pair is only 2.5 eV in Si(Li) and 3.0 eV in Ge(Li) detectors. When a small voltage is applied across a semiconductor detector, a high-energy photon will interact with the detector and liberate electrons leaving a positive hole in the lattice structure. Under an applied electric field, both the electron and the positive hole will move towards opposite electrodes

inducing an electric current. Since the size of the electrical signal is relatively large and proportional to the radiation energy absorbed, semiconductor detectors are useful for energy-selective radiation counting.

Both, Ge- and Si-based semiconductors conduct a significant amount of thermally induced electrical current at room temperature. Therefore, it is necessary to operate and maintain these detectors at relatively low temperatures. High-purity germanium (HPGe), however, needs to be cooled to low temperatures, while others such as cadmium telluride (CdTe) and cadmium zinc telluride (CZT) operate at room temperature. Ge(Li) and Si(Li) detectors are relatively inefficient for detecting high-energy gamma photons. Both, CdTe and CZT have stopping powers similar to NaI(Tl) scintillation detectors. Even denser semiconductors, such as lead iodide (PbI) and thallium bromide (TlBr), are currently under development and may be useful for detecting high-energy photons. CdTe and CZT are also available as pixelated detector arrays with a typical intrinsic spatial resolution of 2.4 mm.

6.2.2 Scintillation Detectors

When high-energy photons interact with the atoms of a scintillation crystal, the electrons are raised from a *valence band* or an orbital to a forbidden, unfilled *conduction band* of a higher energy state. The excited atoms quickly return to the ground state emitting a visible light in a process known as *luminescence*. The number of electrons raised to a higher energy level, and the consequent number of visible light photons emitted by the crystal, depends on the energy of the incident photon. The photoelectric effect is the primary mode of interaction of photons with the atoms in the crystal. The visible light emitted by the crystal is usually in the ultraviolet range. For the crystal to emit light in the visible range (400–500 nm), an alkali halide crystal, with an impurity of (<1%), such as thallium iodide, must be *activated* (or *doped*). The scintillation photons produced by the luminescence are emitted *isotropically* (in all directions) from the point of interaction. The most important scintillators used in current PET and SPECT scanners are the following:

Sodium iodide doped with thallium iodide (NaI(Tl)
Bismuth germanate, $Bi_4Ge_3O_{12}$ (BGO)
Lutetium oxyorthosilicate doped with cerium, Lu_2SiO_5:Ce (LSO)
Yttrium oxyorthosilicate doped with cerium, Y_2SiO_5:Ce (YSO)
Gadolinium oxyorthosilicate doped with cerium, Gd_2SiO_5:Ce (GSO)
Barium fluoride (BaF_2)
Lutetium yttrium oxyorthosilicate (LYSO)

The physical properties of several scintillators are compared in Table 6.2. The most important properties of a detector are stopping power, light output, signal decay time, and the intrinsic energy resolution of the crystal. The following points may be noted: (1) The stopping power is characterized by the MFP or attenuation length, which depends on the density (ρ) and effective atomic number (Z_{eff}) of the crystal. A crystal with shorter attenuation length will have higher efficiency and sensitivity. (2) A crystal with high light output (photons keV^{-1} absorbed) will have good energy resolution. (3) A short decay time of the crystal can

Table 6.2 Physical properties of scintillators

	NaI (Tl)	YSO	BaF2	LYSO	GSO	BGO	LSO
Density (g cm^{-2})	3.67	4.53	4.89	5.31	6.71	7.13	7.4
Effective Z	50.6	34.2	52.2	54	58.6	74.2	65.5
Light output (photons/keV)	38	46	2		10	6	29
Relative light output (%)	100	118	5	76	25	15	75
Wavelength, λ (nm)	410	420	220	420	440	480	420
Decay time (ns)	230	70	0.6	53	60	300	40
Attenuation, μ (cm^{-1}) at 511 keV	0.3411	0.3875	0.4545	–	0.6978	0.9496	0.8586
Attenuation length (1/μ)	2.93	2.58	2.20	2.0	1.433	1.053	1.169
Photoelectric/Compton ratio	0.22	–	0.24	–	0.35	0.78	0.52

help process each pulse separately at higher counting rates with minimum dead time. (4) A crystal with better energy resolution can reject scattered photons more effectively. The overall scanner spatial resolution, however, depends on several other factors.

With NaI(Tl) crystal, the detection efficiency for 140-keV photons is >90%, but for 511-keV photons the efficiency drops to <10%. The intrinsic energy resolution of the crystal is more important for SPECT scanners, while the stopping power of the crystal is one of the main considerations in the choice of the crystal that can interact with 511-keV photons in PET scanners. With the current PET scanners, BGO and LSO are the preferred crystals, while NaI(Tl) is the only crystal that is used in all the major clinical SPECT scanners. A number of other scintillators such as CsI(Tl) and CsI(na) are also under evaluation. The technology of PET and SPECT scanners is continously evolving and is dependent on many other factors besides scintillators.

6.2.2.1 Photodetectors

One of the common characteristics of all scintillators is that following interaction with high-energy photons they all produce a very weak signal of visible light, or a scintillation photon. The purpose of a photodetector is to convert a scintillation photon with 3–4 eV energy into an electrical current. The probability of converting a photon into an electron is called *quantum efficiency*. The two categories of photodetectors used are photomultiplier tubes (PMTs) and semiconductor-based photodiodes.

A PMT is a vacuum tube that consists of an entrance window, *photocathode*, followed by a series of *dynodes* (electrodes), each of which is held at a greater voltage with a resistor chain. The scintillation photon strikes the photocathode and release photoelectrons, which are then accelerated to the first dynode and release even more electrons, which are then accelerated to the next dynode. After passing a series of dynodes, the number of electrons is amplified to $>10^6$, producing a sizeable current in the milliampere range at the anode. Despite of their bulkiness, almost all commercial PET and SPECT scanners use PMTs because of their high gain or amplification, ruggedness, and stability. The quantum efficiency of the photocathode in PMTs is about 15–25%. In order to improve this efficiency, more advanced PMTs, known as position-sensitive (PS) PMTs and multichannel (MC) PMTs, are under development and evaluation.

A photodiode consists of a thin piece of doped silicon wafer (a couple of hundred micrometers thick). The principle of operation is the same as that of a semiconductor. The quantum efficiency (60–80%) of photodiodes is much better than that of PMTs, but the signal of the electrical current is very weak because photodiodes do not have internal amplification or gain. In order to improve the signal-to-noise ratio (SNR), a new type of photodiode known as *avalanche photodiode* (APD) has been developed, which has an internal amplification, however it is still not as good as that of PMTs.

6.2.2.2 Radiation Detector Performance

Spectroscopy is the study of the energy distribution of a radiation field. Most spectrometers are operated in the pulse mode and the amplitude of each pulse is proportional to the energy deposited by the interaction of the photon with the crystal. The amplitude, however, may not be proportional to the total energy of the incident photon. A *pulse height spectrum* (Fig. 6.3) represents the number of interactions or counts per minute (cpm) as a function of the energy of the photon, but it is not the same as the actual energy spectrum of the incident radiation. The performance characteristics of radiation detectors can be expressed quantitatively using parameters, such as *sensitivity* and *energy resolution*.

Sensitivity (or *efficiency*) is the detected count rate per unit of radioactivity. *Geometric sensitivity* of a detector is the fraction of emitted photons that reach the detector, whereas the *intrinsic sensitivity* or the *quantum detection efficiency* (QDE) is the fraction of those photons that reach the detector which are actually detected. For example, 1 μCi of ^{99m}T has 2.2×10^6 disintegrations per minute (dpm), and each decaying atom produces one 140-keV photon. If the detector can detect 1.0×10^5 photons, then the sensitivity of the detector is 10%. As discussed previously, various physical characteristics of the crystal (Table 6.2) can affect the sensitivity of the scintillator.

Many radionuclides emit a number of photons (x-rays and γ-rays) of discrete energies. The electrical signal output from a detector–photodiode combination, however, appears as though it is coming from a range of energies

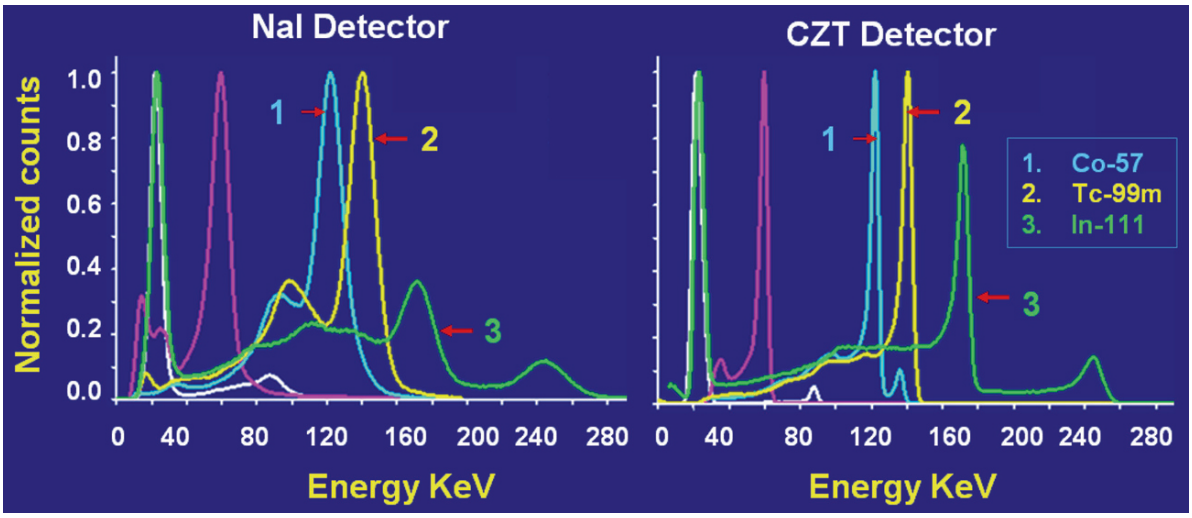

Fig. 6.3 Pulse height spectra of several radionuclides using NaI or CZT detector. The energy resolution with CZT detectors is much higher compared to that with NaI detector

due to the absorption and scattering of the incident photons. Energy resolution quantifies the ability of a specific crystal to differentiate or discriminate photons of different energies. It is expressed quanti-tatively as a percent of full width at half-maximum (FWHM = ΔE) of an energy spectrum (counts detected vs. energy (keV)) of a radionuclide with a specific photopeak energy (E_γ).

$$\text{FWHM}\,(\%) = \frac{\Delta E}{E_\gamma} \times 100 \tag{6.7}$$

For energy-selective detection (as in Anger cameras), the FWHM determines the resolution of the detector. The sensitivity can be increased by increasing the value of ΔE, but that would degrade the resolution.

6.3 Radionuclide Imaging Systems

The purpose of radionuclide imaging is to obtain an image of the in vivo distribution of a radiotracer on the basis of the external detection of high-energy photons emitted by the radionuclide. In the 1940s, attempts were made to detect the distribution of radioactivity in vivo, but only in the 1950s, that in vivo radionuclide imaging became a practical clinical modality, due to the introduction of the rectilinear scanner, by Ben Cassen. In the 1950s, Hal Anger developed the first γ-ray camera using a single, large-area NaI(Tl) scintillation crystal coupled to PMTs. This camera, subsequently, called the *Anger scintillation camera*, has become the predominant molecular imaging device in nuclear medicine. Since then, many refinements and modifications have been made to improve the image quality of this camera.

Conventional Anger camera images compress the three-dimensional (3D) distribution of the radiotracer into a two-dimensional (2D) image. As a result, the contrast between areas of interest and the surrounding territory is often significantly reduced. In *planar imaging* systems, the radiation from a source (patient) is collected and the data is presented as though all photons are coming from a single plane. In a patient, images of a specific area of interest at one depth are obscured by images of structures above and below the area of interest. *Tomography* simply means an image of a slice. Tomographic images are 2D representations of structures lying within a selected plane or depth in a 3D object. *Computed tomography* (CT) techniques are based on rigorous mathematical algorithms initially developed by Radon, in 1917. The introduction of CT, in the 1970s, helped to implement CT techniques to the radionuclide imaging methods. X-ray CT is a transmission CT since x-rays from an external source are transmitted through the patient to a detector. With radiotracers, high-energy photons are emitted from the patient; this technique is called *emission computed tomography* (ECT). Since radionuclides emitting γ-rays, are used for imaging, the technique is also called *single photon emission tomography* (SPECT). With positron-emitting radionuclides, the imaging technique is called *positron emission tomography* (PET).

6.3.1 Anger Camera

The Anger gamma camera consists of a single rectangular NaI(TL) crystal (~50–60 cm in area) optically coupled to a large number of PMTs (typically 37–91). While the thickness may vary from 0.25 in. (~6 mm) to 1 in. (~25 mm), most cameras are made up of a 3/8 in. (~10 mm) crystal for optimum performance of radionuclides with energies between 120- and 200-keV photons. Thinner crystals have better spatial resolution, but lower sensitivity.

A *collimator* (usually made of lead) with holes (round, square, rectangular, or hexagonal) allows high-energy photons coming from the patient in a specific direction to enter and interact with the crystal. The walls, called *septa*, around the holes in the collimator absorb photons that are traveling in an oblique angle to the axes of the holes. In other words, the collimator controls the direction of the photons entering the crystal. The thickness of the collimator and septa as well as the number of holes determines the overall sensitivity and resolution of the Anger camera. Most cameras have a wide choice of parallel hole collimators such as "low-energy high sensitivity," "low-energy all purpose (LEAP)," "low-energy high resolution," medium-energy, high-energy, and ultrahigh-energy collimators, each designed to optimize a specific imaging study. With all parallel-hole collimators, the spatial resolution degrades rapidly as the distance (space) between the patient and the collimator increases. A pinhole collimator, consists of a small hole (3–5 mm in diameter) in a piece of lead or tungsten, and is commonly used to produce magnified views of small objects. The magnification and sensitivity, however, decrease as an object is moved away from the pinhole.

Following interaction of photons with the crystal, the emitted light photons induce electrical signals in the PMTs. The PMTs closest to the scintillation even in the crystal receive more light than those that are most distant and as a result produce a larger electrical signal. The relative amplitude of these pulses determines the location of the interaction in the crystal and the exact location of the origin of the photons coming from the patient. The electrical pulses from PMTs pass through preamplifiers and ADCs (analog-to-digital converter). The digital X, Y, and Z signals are corrected using correction circuits, followed by energy discrimination using SCAs (single-channel analyzers). The signals are finally converted into digital images in a computer.

6.3.1.1 Anger Camera Performance

The measures of performance of a scintillation detector or camera alone are called *intrinsic* measurements, while the measures with the collimator are called *extrinsic* or system measurements; these measurements give the best indication or clinical performance.

Uniformity is a measure of the camera's response to uniform irradiation of the detector surface.

Spatial resolution is a measure of the camera's ability to accurately assess the spatial variations in radioactivity concentrations that are in close proximity, and to distinguish these areas as separate radioactive objects or source regions. A systems spatial resolution is normally determined by obtaining a *line spread function* (LSF) using a line source (capillary tube) of radioactivity. FWHM and *modular transfer function* (MTF) are derived from the LSF. On the basis of the system spatial resolution (R_s) and intrinsic resolution (R_i) of the detector, the collimator resolution (R_c) can be estimated using the following equation.

$$R_s = \sqrt{R_c + R_i} \tag{6.8}$$

Spatial linearity is the ability of a camera to, accurately, depict the true shape of the object. Any distortion of the shape is an indication of spatial nonlinearity.

The *system sensitivity* or *efficiency* (E_s) of a camera is the fraction of photons emitted by a source that produce counts in an image. It is the product of the intrinsic efficiency of the crystal (E_i), the collimator efficiency (E_c), and the fraction (f) of interacting photons accepted by the pulse height analyzers. The *photopeak efficiency* is defined as the fraction of photons reaching the crystal and produce counts, which represent the photopeak in the energy spectrum:

$$E_s = E_i \times E_c \times f \tag{6.9}$$

The *energy resolution* of an Anger camera is a measure of its ability to distinguish between the different energies of photons that are interacting with the crystal. A camera with good energy resolution can produce images with better *contrast* since it can reject scattered photons with lower energies. *Multiple energy (or window) spatial registration*, on other hand, is the ability of a camera to maintain the same magnification, regardless of the photopeak energy of the incident photons.

In a NaI(TL) crystal, approximately one visible photon is emitted for every 25 eV of energy deposited.

For example, when a 140-keV photon deposits all of its energy in the crystal, it will generate 5,600 visible light photons, of which only 20–25% may eject electrons from the photocathode and contribute to the signal from the PMT. The intrinsic efficiency (E_i) of the camera is determined by the thickness of the crystal and the energy of incident photons. With gamma cameras, there is a design compromise between the intrinsic efficiency (E_i) and the intrinsic resolution (E_s) since thinner crystals have better resolution, but lower sensitivity and, vice versa. The compromise between the collimator efficiency (E_c) and the collimator resolution (R_c) is the most important and significant an limitation of Anger camera performance. The systems spatial resolution (R_s) degrades (FWHM increases) as the collimator-to-object distance increases, without any significant impact on the system efficiency (E_s).

With many of the Anger scintillation cameras (with a 3/8 in. crystal), the intrinsic spatial resolution (R_i) for 140-keV photons of ^{99m}Tc is between 2.7 and 4.0 mm. With a parallel-hole collimator, however, the system resolution (R_s) could dramatically decrease to 8–12 mm at a distance of 10–20 cm from the collimator surface. The most important point is that the system resolution is not the same in the entire filed of view.

6.3.1.2 Planar Image Acquisition

Planar images with gamma cameras can be acquired either, in a *frame* mode, or a *list* mode. In a frame mode, an image is formed as the acquisition is in progress, whereas in a list mode, the images are created subsequently at the end of an acquisition.

The frame-mode acquisition is the most common method. Planar frame-mode acquisitions can be *static*, *dynamic*, or *gated*. In a static planar image acquisition, a single image (one frame) is obtained either for a preset time interval (such as 5 or 10 min) or for a total number of counts (such as 0.5 or 1 million counts). In a dynamic image acquisition, a series of images (many frames and each frame/specific time) is acquired one after another to follow the time–activity distribution of radioactivity in a specific organ or area of interest. In gated acquisition, each frame is acquired on the basis of a physiological trigger such as an electrocardiogram (ECG). Each image consists of many *pixels*, and each pixel stores the acquired counts. Common image formats are 56 × 56, 128 × 128, 256 × 256, or 256 × 1,028 (whole-body scans only). In the *byte mode* (8 *bits*), each pixel stores 255 counts, while in a *word mode* (2 bytes), each pixel can store 65,535 counts. As discussed earlier, the planar projection image depicts 2D projections of 3D distribution of radioactivity in a patient. In an ideal projection image, there is no attenuation of photons within the patient and also there is no degradation of the image resolution by the camera. Since planar images are not corrected for attenuation, and the resolution is not same at different depths, planar imaging studies are not ideal projection images.

6.3.1.3 SPECT Image Acquisition

The conventional tomography, also called *focal plane tomography*, is based on scintillation detectors with focused or converging collimators. Structures close to the focal plane are in focus and well resolved, while the structures out of plane are not removed from the images, but blurred by an amount proportional to their distance from the focal plane. In contrast, the SPECT technique is based mainly on parallel-hole collimators. The standard planar projection images acquired in many angles around the patient are processed or reconstructed mathematically to obtain an image of a slice, and the overlying structures are removed completely from the image of each of the contiguous slices. One of the most important assumptions in SPECT imaging studies is that the distribution of radioactivity in the body remains constant throughout the duration of the scan.

Most routine clinical SPECT imaging systems are based on dual-head fixed 180° or variable angle cameras and triple-head variable angle cameras. Standard projection images are acquired in a frame mode and 64^2 or 128^2 format, either in a "step and shoot mode" or while the heads are moving continuously. As mentioned earlier, since these projections images are not ideal, images are generally acquired over a complete revolution (360°). For cardiac studies, optimal imaging protocols require projection images acquired only over a 180° arc around the patient. While older SPECT systems followed circular orbits around the patient, current SPECT systems have been designed to provide both circular and noncircular (body contouring) orbits.

The projection images are first corrected for nonuniformities and axis-of-rotation misalignments.

Fig. 6.4 SPECT/CT systems in routine clinical use

Table 6.3 Commercially available SPECT/CT systems

	Infinia Hawkeye	Precedence	True point
Manufacturer	GE Healthcare	Philips	Siemens
SPECT system	Infinia	Skylight	Symbia
CT system	Hawkeye	Brilliance	T, T2, T6
No. of CT slices	1 or 4	6 or 16	2 or 6
Slice thickness (mm)	10 or 5	0.6–12	0.6–10*
Tube rotation (s)	23	0.5	0.6–1.5*
Standard HC resolution (lp/cm) (2% MTF)	.3	13	15*
Room dimensions (cm)	470 × 711	442 × 640	358 × 419

*Values are for Symbia T6 (see text)

HC high contrast; *lp/cm* line pairs per centimeter; *MTF* modulation transfer function

Subsequently, the images are mathematically processed to reconstruct transverse images using either filtered backprojection, or iterative methods.

Since high-energy photons traverse long paths through the patient, attenuation effects are more severe in body SPECT than in brain SPECT. In addition, attenuation is not uniform throughout the patient. Therefore, standard methods of attenuation correction based on the assumption of uniform attenuation may not be applicable for SPECT studies. Several commercial SPECT systems use radioactive sources (such as ^{153}Gd) to generate transmission scans while acquiring the projection images. In the last 3–5 years, several SPECT/CT systems (Fig. 6.4 and Table 6.3) have been introduced primarily for coregistering anatomic and functional SPECT images. CT scans may also offer an opportunity for the development of attenuation–correction methods. Attenuation–correction methods for clinical SPECT studies, however, are still under evaluation.

In SPECT studies, spatial resolution deteriorates as the radius of the camera orbit (body to collimator distance) increases. Brain SPECT produces images of better resolution than body SPECT. Also, noncircular body contouring orbits produce better resolution images than circular orbits. Compared to planar imaging, SPECT, in general, produces images with lower resolution for several reasons. In order to increase sensitivity, SPECT images are, generally, acquired with lower resolution parallel-hole collimators. Collimators are very inefficient, and allow only 1 in 5,000 photons that hit its surface to be transmitted through to the detector, and therefore, are the limiting component of count sensitivity and spatial resolution. Further, the distance between the body and the collimator is greater with SPECT. Since many projection images are obtained, counts/frame is much less with SPECT. SPECT images, however, do provide better contrast and reduced structural noise since the activity in the overlapping tissues is completely eliminated.

6.3.1.4 New Cardiac SPECT systems

Several clinical SPECT systems have been optimized for cardiac imaging. Some of these systems are still based on conventional dual-detector γ-camera systems, but the size of the systems were minimized to occupy less space. Three new systems have been introduced with certain new and novel technological advancements.

The Cardius system (Digirad) is available with up to three detector heads based on pixelated CsI(Tl) crystals. In this system, the detectors remain stationary and the projections are collected as the patient, sitting upright in a chair, is rotated. The other two clinical SPECT systems are based on semiconductor detector technology. The CardiArc has a 180° arc of pixelated CZT detectors with a series of lead plates (slats) to provide axial collimation for the detectors. A curved lead plate with a set of slits is located in front of the slats. The combination of the slits and slats, in addition to the motion of the slit plate, provides pinhole sampling with relatively high count sensitivity and better spatial resolution, compared to conventional SPECT systems. The D-SPECT system, on the other hand, consists of ten individual collimated pixelated CZT modules. Once the location of the heart has been determined, the CZT detector modules independently rock back and forth to acquire the data for the projection images. No gantry rotation is necessary. This system has both higher sensitivity and twofold improvement in spatial resolution compared to any conventional clinical SPECT system.

One of the major advantages of SPECT systems based on pixilated CZT modules is that it is now possible to image radiotracer distributions where the activity changes monotonically in a specific region of interest, during acquisitions. As a result, it is possible to derive additional information about the kinetics of the radiotracer distribution. With dynamic SPECT, it is possible to model the kinetics of distribution into the reconstruction algorithm to yield sequential time-sampled tomographic images. With its superior spatial resolution and high sensitivity, coupled with the ability to perform dynamic SPECT, the SPECT imaging technique provides new opportunities to perform molecular imaging studies with radiotracers based on ^{99m}Tc, ^{123}I, and ^{111}In.

In a recent review article, Mark Madsen (2007) concludes that "SPECT continues to progress with major improvements in instrumentation and reconstruction. The limits of spatial resolution and sensitivity have not yet been reached either for clinical devices or for small-animal imagers. Improvements in detector technology and image-forming apertures will yield intrinsically better projection information. At the same time, refinements in corrections for scattered radiation, attenuation, and spatial resolution losses will result in more accurate and quantitative reconstructed tomographic slices. The capability for combining this information with correlative imaging, both anatomic and functional, from other modalities is also expected to improve."

6.3.2 PET Scanners

PET scanners were designed to obtain in vivo images of the distribution and uptake of radiotracers on the basis of positron emitting radionuclides. A typical PET scanner consists of many rings of scintillation detectors which surround the subject. Following the interaction of the positron with the tissue, two annihilation photons (511 keV) are emitted, isotropically. The PET scanner uses the annihilation coincidence detection (ACD) method to obtain projection images of the radiotracer distribution. The images are first corrected for attenuation, scatter, etc. and then mathematically processed, as in the case of CT and SPECT, to obtain transverse images of several slices of the body in a given field of view (FOV). A number of reviews have been published, describing the historical development of the PET technology (Nutt 2002). The basic design, principles of operation, and performance characteristics of clinical PET, PET/CT, and MicroPET scanners are discussed in this section.

6.3.2.1 Positron Annihilation and Coincidence Detection

A positron ejected by a radionuclide travels a very short distance in a tissue, dissipating its kinetic energy in collisions with electrons, and finally combines with an electron to form a positronium, a state which lasts for a very short time (10^{-10} s). The subsequent positron–electron annihilation results in the emission of two 511-keV photons, 180° apart. A PET scanner is designed to detect this pair of annihilation photons almost simultaneously on the basis of a process known as *annihilation coincidence detection* (ACD), which establishes the trajectories of detected photons or lines of response (LOR). ACD only establishes the location of an annihilation event within the LOR; the exact location of a positron emitting radionuclide, however, is determined mostly using the CT techniques, based on mathematical processing of millions of LOR to generate a computed tomogram of the PET tracer distribution. In a different approach, known as *time of flight* method, measuring the difference in arrival time

of the two annihilation photons at the opposite detectors helps to determine the exact location *d* of the annihilation event along the LOR.

Positron Range and Noncolinearity

Determining the exact LOR along which a positron emitting radionuclide can be found is one of the major factors that determine the spatial resolution of a PET scanner. *Positron range* and *noncolinearity* are two effects that may lead to errors in determining the LOR.

Positron emitting radionuclides differ in the energy of emitted positrons. For example, the energy of positrons emitted by ^{18}F (E_{max} = 0.63 MeV) is almost one-fifth that of a positron emitted by ^{62}Cu (E_{max} = 2.93 MeV). The positron range is the direct distance traveled by the positron from the decaying atom to the exact location of the annihilation event. The positron range is a function of the energy of positron (Fig. 6.5). The mean positron range may vary from a fraction of a millimeter to 4–6 mm, depending on the radionuclide. The error due to the positron range may be significant and, therefore, this range limits the ultimate resolution attainable by PET. It is very important to appreciate the fact that the SPECT technique inherently offers no limitation in spatial resolution due to photon energy, while the PET technique has a theoretical limit in terms of spatial resolution.

In contrast to the positron range, noncolinearity is independent of the positron emitting radionuclide. The positron and electron are not exactly at rest when the annihilation occurs. As a result, the two annihilation photons differ in their momentum, and are not emitted exactly at 180° apart (they may be emitted with a distribution of angles around 180° (typically ±0.25°)). For a given PET scanner with diameter *D*, this blurring effect, due to noncolinearity (Δ_{nc}), can be estimated as follows:

$$\Delta_{nc} = 0.0022 \times D \text{ (in mm)} \qquad (6.10)$$

With most clinical PET scanners that have a ring diameter of approximately 80 cm, the blurring due to a noncolinearity error may be 1.76 mm. However, in MicroPET, this effect is somewhat less significant.

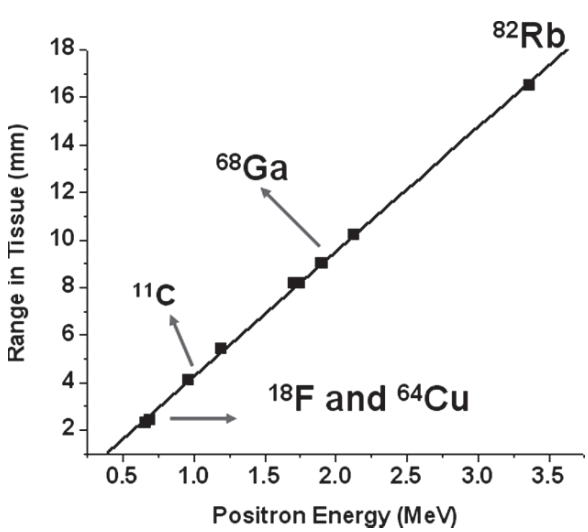

Fig. 6.5 The positron range in tissue as a function of positron energy

Coincidence Event Types

A *true coincidence* is the simultaneous interaction of a pair of photons (511 keV) resulting from the annihilation of a positron-eletron pair (Fig. 6.8). A *random coincidence* occurs when two 511-keV photons from separate annihilation events, that occurred as a result of the decay of different atoms, strike the opposite detectors, simultaneously. In the tissue, the 511-keV photons undergo scatter and lose some energy. A *scatter coincidence* occurs when one or both of the 511-keV photons from a single annihilation event are scattered, but detected, simultaneously, by the opposite detectors. The total number of events (true, random, and scatter) detected by the coincidence circuit in a PET scanner is referred to as *prompt coincidences*. Also, when 511-keV photons or the scattered photons are detected, they are referred to as a "singles." Since photons travel at the speed of light (30 cm ns^{-1}), the detection times of a pair of photons by the coincidence circuit can be between 2 and 3 ns. Typically, a coincidence timing window (τ) of 6–12 ns is used to account for statistical fluctuations in timing the detection events.

6.3.2.2 Pet Scanner Design

Since the early 1970s, several different PET detector configurations have been developed. In most dedicated PET scanners, pixilated or multicrystal detectors are arranged in rings or polygonal arrays completely encircling the patient. In addition, two or three planar large-area detectors (as in Anger camera) are also used to configure the PET scanner. The majority of current

Fig. 6.6 The typical PET scanner with ring detector configuration

clinical PET and MicroPET scanners, however, are based on the full-ring configuration (Fig. 6.6). Scintillation crystals coupled to PMTs are used as detectors. Compared to full-ring detectors, the efficiency of other detector configurations for coincidence detection is significantly poor (<30%). A PET scanner typically consists of several components:

- Detector consisting of a scintillator coupled to PMTs
- Collimator
- Signal processing electronics
- Coincidence circuit
- Data-acquisition computer
- Reconstruction, display, and image analysis systems

The basic principles of a PET detector and collimation are discussed below. The electronics associated with the signal processing and the computer hardware needed for data acquisition, image processing, etc. are highly technical and are discussed in detail in many other publications (Nutt 2002; Townsend 2008; Seo et al. 2008).

Block Detector

The detectors in a PET scanner perform much more efficiently than those in a gamma camera. The relatively thin NaI(TL) crystal in the gamma camera detects many photons, simultaneously. In contrast, each of the pixilated scintillation crystal elements in the PET scanner detects one photon at a time and, hence, is more efficient. In order to detect the annihilation photons in PET, the scintillator needs be thick and should have a greater stopping power to interact with the 511-keV photons. In addition, the crystals should have relatively good light output and a short time constant to reduce random coincidences and dead time. Compared to the NaI(Tl) crystal, those of BGO or LSO detect significantly more (80%) of the incident 511-keV photons and, therefore, are the most common crystals used in PET scanners. GSO and BaF_2 also have suitable properties for use in PET scanners. The important properties of scintillators used in PET are given in Table 6.2.

In early PET scanners, each scintillation crystal was coupled to a single PMT, and the size of the crystal largely determined the spatial resolution of the PET scanner. Smaller crystals were needed to improve the resolution. Since the size of PMT is relatively large, it was difficult to couple one PMT for each of the small crystals. In the 1980s, a multicrystal, two-dimensional BGO *block detector* system was developed (Nutt 2002). The majority of dedicated clinical PET scanners in use today are based on the block detector design. A schematic of the block detector is shown in Fig. 6.7.

A block of scintillation detectors is made by segmenting (cutting or channeling) a relatively large block of crystal (typically, 4 × 4 in area and 3 cm deep) into an 8 × 8 or 6 × 6 array (Fig. 6.7). The channels are filled with a light-reflective material to prevent conduction of light from each crystal element to the next in the block. The scintillator block is then coupled to four PMTs and requires a high voltage (1,600–1,800 V) supply. Most PET scanners consist of 144–288 block detectors and contain 10,000–20,000 detector elements.

An alternative to the block detector design is the pixelated detector matrix, wherein individual small-area detector elements (typically 4 × 6 mm in area and 20 mm in depth) are fixed onto a continuous light guide, backed by a close-packed array of PMTs. In order to reduce the depth-of-interaction effect and improve the resolution, a combination of two crystals such as BGO and LSO, known as *phoswich*, has been developed, but not yet used, routinely, in PET scanners.

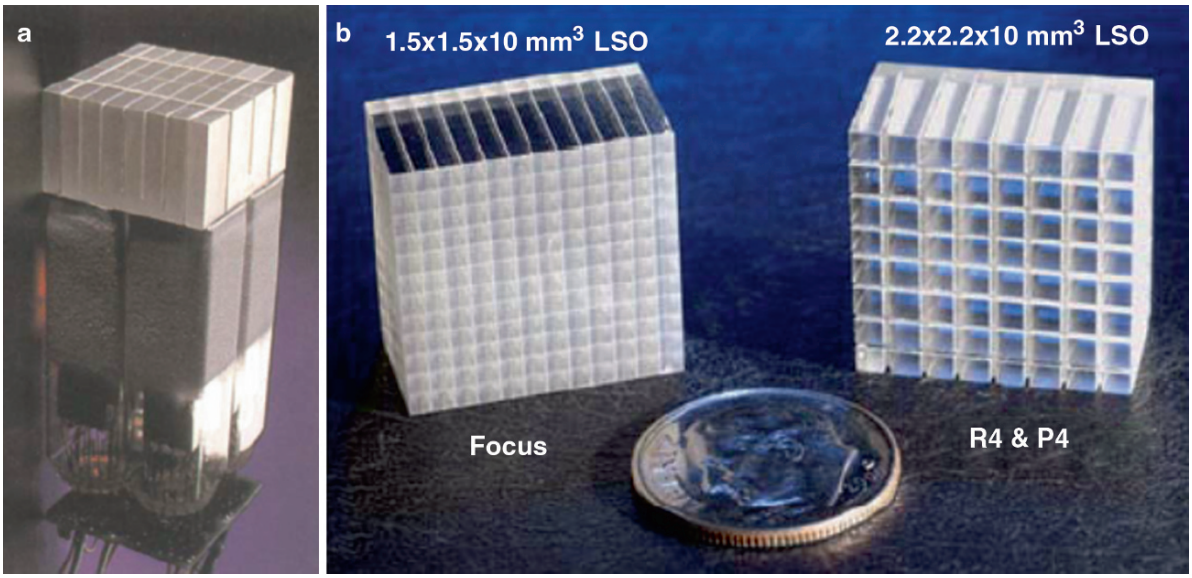

Fig. 6.7 The "block" detector (**a**), and Crystal arrays (**b**) used in the construction of microPET scanners (Levin 2005)

Collimation in PET

There are two kinds of collimation used in PET: one to direct the photons to the detector and the other to select the detected events. Thick lead rings are used to define the external axial FOV, while thin lead or tungsten rings (1–5 mm thick) (usually referred to as septa) are employed to define the individual imaging planes. These septa can be positioned to define the slices during 2D PET studies, but can be retracted during 3D PET acquisition, to increase sensitivity.

The electronic circuit of ACD provides the *electronic collimation* by selecting only those counts that are simultaneously detected by the opposite detectors, during the coincidence timing window. Typically, electronic collimation selects only 1% of the singles as prompt events for further processing, while the remaining 99% are rejected.

6.3.2.3 PET Data Acquisition

Most PET scanners have a data-acquisition computer system (DACS), which generally requires very large random access memory, approximately 500–1,000 mb. Reconstructing PET images is a very computation-intense task and, therefore, special purpose computers, called *array processors*, are used.

In order to obtain an in vivo PET image of a radiotracer distribution, the data acquisition involves obtaining two different scans; a transmission and emission scan, while the patient is in the scanner. In addition, two other scans, called *blank scan* and *normalization scan*, are necessary to process and reformat the PET projection data into a quantitative PET scan, with multiple slices.

Transmission Scan

In order to obtain a true quantitative PET image, the emission scan must be corrected for the attenuation of a pair of coincidence photons within the body. *A transmission scan*, in PET, is usually performed to correct for attenuation of the 511-keV photons in the body. With the object in the FOV, a transmission scan is performed using an external (transmission) rod source of activity or a CT scan. The probability of attenuation for each LOR can be determined by comparing the count rate from the transmission source, while the patient is in the FOV, with the unattenuated count rate from the same transmission source, when the patient is not in the FOV (referred to as *blank scan*).

With older PET scanners and several MicroPET devices, a transmission scan is first obtained by using external rod sources of radiation. The most common rod source is based on long-lived ^{68}Ge ($T_{½}$ = 270 days),

which decays by EC to ^{68}Ga that decays by emitting a positron. To improve counting statistics, some clinical PET scanners use ^{137}Cs ($T_{½}$ = 30.1 year), which emits a 662-keV gamma photon some MicroPET scanners use ^{57}Co ($T_{½}$ = 270 days), which emits a 120-keV gamma photon. In either case, the attenuation of 511-keV photons is estimated on the basis of the energy of photons used for the attenuation correction. Typically, transmission scans using rod sources ^{68}Ge or ^{137}Cs are performed prior to the administration of PET radiotracer. A good-quality transmission scan generally takes 20–30 min.

A blank scan (with no object in the FOV) must be completely noise free and is generally performed for 1 h or, at least 10 times the duration for which the emission scan is obtained. The blank scan is obtained using a rod source or CT scan depending on the technique used for the attenuation correction.

With the current PET/CT scanners (Fig. 6.8 and Table 6.4), the most common method for attenuation correction is based on the CT scan. A nondiagnostic CT scan can be used as a transmission scan. Since the CT scan is based on lower energy (~60-keV) X-ray photons, the CT scan can be performed either before or after the administration of a PET radiotracer. In addition, a CT scan for attenuation correction takes only 0.5–2 min.

Emission Scan

2D Vs. 3D PET

Many of the current PET or PET/CT scanners allow the scanner to perform both 2D and 3D imaging. PET scanners that do not have septa always work in the 3D mode only. In the 2D mode, the scanner is relatively insensitive to the scattered radiation and generally considered more quantitative than 3D imaging. In the 3D mode, the efficiency of detection increases by about 5 times, for unscattered photons and by about 20 times, for the scattered photons. Even though the scattered fraction is much higher in the 3D mode, with appropriate scatter correction algorithms there may not be any significant losses in spatial resolution. Three-dimensional imaging is recommended when the injected dose is suboptimal or delayed imaging is preferable to obtain improved contrast. With recent improvements in the 3D reconstruction and image data correcting, most commercial PET scanners are designed to optimize in the 3D acquisition.

PET Imaging Modes

Following the administration of a PET radiotracer into a subject, imaging can be performed in three different modes.

A *dynamic emission scan* is used to obtain PET images in order to study the time–activity distribution of a radiotracer in a specific tissue or organ of interest. Dynamic scans are performed using a series of imaging frames, which get longer as the study progresses. Measurement of blood flow and receptor imaging studies are often performed using dynamic scans. These studies, however, may require arterial or venous sampling to provide an *input function* to estimate quantitative parameters, based on pharmacokinetic modeling of radiotracer distribution.

A *static emission scan* is normally obtained only when the radiotracer distribution is fairly stable or reaches an equilibrium state. The static scan is acquired in a single frame, and it is assumed that the tracer concentration in a given tissue is constant, except for the

Fig. 6.8 PET/CT scanners

Table 6.4 Commercially available PET/CT systems*

	GE Healthcare	Siemens Healthcare	Philips Healthcare
Models	Discovery PET/CT 690 Discovery PET/CT 600 Discovery PET/CT STE16 Discovery PET/CT ST4	Biograph mCT Biograph TruePoint	Gemini TF Big Bore (PET/CT) Gemini TF 64 (PET/CT) Gemini TF 16 (PET/CT) Gemini GXL 16 (PET/CT)
Number of detectors	24 rings	192	28 Pixelar Modules
Number of image planes	47	109	45 or 90
Plane spacing	3.27 mm	2 mm	2 or 4 mm
Number of crystals	12,288 – 13,440	32,448	28,366; 17,864 (GXL 16)
Number of PMTs	256 – 280		
Ring diameter	81 or 88.6 cm	84.2 cm	90 cm
Physical Axial FOW, cm	15.7 cm	21.6 cm	18. cm
Detector material	BGO	LSO	LYSO or Zr:GSO
Crystal size, mm	4.7 × 6.3 × 30 6.3 × 6.3 × 30 (ST4)	4 × 4 × 20	4 × 4 × 22 4 × 6 × 30 (GXL 16)
PET Performance	**For Discovery PET/CT 690**	**For Biograph mCT**	**For Gemini TF Bigbore**
System sensitivity, 3D	76kcps @ 15 KBq/mL	175kcps ≤@ 28 KBq/cc (mCT)	94 kcps @14 KBq/mL And 220 kcps with TOF
Axial resolution at 10 cm, 3D	5.6 mm	5.5 mm	5.2 mm
Transverse resolution at 10 cm	5.6 mm	4.8 – 4.9 mm	5.1 – 5.2 mm or 6.0 mm (GXL 16)

* The data in this table was based on PET/CT systems comparison chart in Imaging Technology News, June 2009

Note: Two PET cameras (no CT) are also available for clinical use: Attrius™ (by Positron) and NeuroPET (by PhotoDetection Systems Inc)

physical decay. The routine FDG-PET scans are performed approximately 1 h post administration of the dose are designed to measure the glucose metabolism in the brain, the heart, and the tumor.

Whole-body emission scan represents a series of static scans performed at different segments or portions of the whole body. The studies are performed in several bed positions by acquiring a static scan for a specific time and then moving the patient (the bed) by a distance that is less than the axial FOV. Most clinical PET scanners have a FOV of 15–20 cm. Typically, five to seven bed positions, each requiring 3–5 min, will complete a whole-body emission scan from head to midthighs in 15–35 min. The data collected at each bed position are subsequently reconstructed into a whole-body volume and can be reoriented into *transaxial*, *coronal*, and *sagittal* views.

6.3.2.4 PET Image Data Correction

In order to produce a quantitative PET image of the radiotracer uptake and localization in various organs and/or tissues, a number of corrections need to be applied to the raw emission scan data, which usually are histogrammed into a 2D matrix and provided as a *sinogram*. In general, the following steps are involved in the generation of a PET image. The sequence of steps 1–3, however, may vary depending on the data-processing software.

1. The emission scan (the emission sinogram) is corrected for random coincidences, scatter, and dead time.
2. An attenuation correction is then applied to the corrected emission sonogram, using the transmission scan (transmission sonogram) and the blank scan.
3. The detector normalization corrections are then applied to the attenuation-corrected PET scan.
4. Finally, the attenuation-corrected PET data is reconstructed to generate a quantitative PET image on the basis of the filtered back projection (FBP) technique or iterative reconstruction algorithms.

Random and Scatter Coincidence Correction

As discussed earlier, the prompt count rate or the measured count rate (N) includes, the true (T), random (R), and scattered (S) counts. Therefore, to obtain the true count rate associated with any LOR, the noise due to

random and scatter counts must be removed from the measured count rate to preserve the image contrast, improve quantitation, and prevent artifacts in the final PET image.

$$T = N - R - S \tag{6.11}$$

In clinical brain PET studies, the ratio of the randoms to true count rate may only be <0.2, but this ratio may even be >1 for whole-body imaging. In general, the random count rate increases with increasing activities in the FOV and also with increases in the duration of the coincidence timing window (τ). If the counting rates for the two detectors in the coincidence circuit are C_{s1} and C_{s2}, then the random count rate R for these detectors is given by

$$R = 2\tau\, C_{s1}\, C_{s2} \tag{6.12}$$

In general, the randoms can be decreased by using thick septa in the 2D mode. Also, by using faster scintillators, such as LSO, one can use a shorter timing window. To correct for randoms, the count rate is first estimated and then subtracted from each point in the sinogram. As shown in the above equation, on the basis of a single rate for each detector and the timing window, one can estimate the random count rate. Another approach is to use two timing windows, one for prompt counts and another that is delayed in time, such that the detector pair cannot measure any true coincidences.

In contrast to the randoms, the scatter coincidence count rate is independent of both the activity in the FOV and the coincidence timing window. Since the scattered photons can only be identified on the basis of the energy of scattered photon, correction for scatter is probably the most difficult to achieve, in PET. More specifically, because most PET scanners operate with a relatively large energy window between 350 and 650, it is difficult to separate scatter events from the primary, unscattered photons. Two-dimensional PET acquisition is the best way to reduce scatter since the thick septa absorb some of the scattered photons. The scattered fraction in 2D brain images may be <0.2, and this fraction may increase up to 0.4. Compared to lead, tungsten septa may help reduce scatter significantly. The 3D PET significantly increases the contribution of scatter events even in brain imaging studies. Since the scatter increases with depth, scatter correction, however, may be of less importance in MicroPET studies of rodents.

Several scatter correction methods, based on analytical, dual-energy window, and simulation methods, have been developed. The discussion of these methods is given in detail in several other publications. Since scatter and attenuation are one and the same phenomenon, scatter can be estimated on the basis of emission data and the attenuation map. Scatter can then be simulated using analytical models or Monte Carlo simulation techniques.

Dead Time Correction

Each detector element in the PET scanner can record only one photon at a time. If another photon interacts with the crystal, while the crystal is still scintillating due to the prior interaction, both the energy and position of both photons will be incorrect. The minimum time needed to process each interaction is about one microsecond (1,000 ns) with BGO and 200 ns with LSO detectors. If the singles count rate is several hundred thousand counts per second, the detector's linear response will be compromised, significantly. Dead time represents the time during which the detector is unavailable to respond to the photon interaction. This parameter characterizes the counting behavior of the system at high count rates.

At low activity concentrations, the measured count rate (cps) follows the ideal linear response. However, as the activity concentration is increased, the observed count rate significantly decreases, depending on the dead time characteristics of the detector system. The most common way to characterize dead time is to fit the scanner response (measured count rate) using either a paralyzable or nonparalyzable dead time model. The paralyzable dead time model predicts that at higher concentrations, there is a gradual and significant decrease in the measured count rate, whereas the nonparalyzable dead time model predicts that at higher activities, the measured count rate gradually increases, but does not represent a linear response. Another problem associated with the dead time limitation is that, at higher activity concentrations, pulse pile-up can become a limiting factor and may contribute to degradation in resolution, and may even introduce artifacts.

Attenuation Correction

As discussed earlier, attenuation and scatter are manifestations of the same physical process. Correction for attenuation involves first removing the scattered events from LORs and then correcting each LOR for the fraction of events that were attenuated from that LOR. The problem of correcting for attenuation in the body is to determine the probability of attenuation for all sources lying along a particular LOR. The measurement of attenuation in PET is completely independent of the isotope distribution, and the location of the annihilation event along the LOR is given by

$$\text{Attenuation} = e^{-\mu d_1 + \mu d_2} = e^{-\mu D} \tag{6.13}$$

For simple extension of the above equation can be made to a case of nonuniform attenuation. For example, μ changes along the LOR as the photon passes through different tissues, such as normal tissue, fat, or bone.

$$A = e^{-\int_0^D \mu(l)dt} \tag{6.14}$$

For a patient, the above equation can be used to obtain a measure of the attenuation of 511-keV photons for a specific section or the whole body by obtaining a transmission scan.

The measured attenuation matrix as a ratio sinogram $R(r, \beta)$ is created by dividing the blank scan sinogram $B(r, \beta)$ by the transmission scan sinogram $T(r, \beta)$. The natural logarithm of this ratio sinogram will result in an attenuation sinogram $A(r, \beta)$ as shown by the following equations:

$$R(r, \beta) = \frac{B(r, \beta)}{T(r, \beta)} \tag{6.15}$$

$$A(r, \beta) = \ln\left(\frac{B(r, \beta)}{T(r, \beta)}\right) \tag{6.16}$$

The attenuation correction of the PET emission data is performed by multiplying the emission sinogram with the attenuation sinogram. This operation is performed on every element of the sinogram.

When a CT scan is used for the attenuation correction, the CT images are normally calibrated in Hounsfield units and must be converted to μ values. These μ values, based on low-energy X-ray photons, do not scale linearly with the 511-keV annihilation photons. In order to deal with these problems, the CT images are segmented into a discrete set of tissue types, which can be treated by applying an empirical scaling factor that scales the corresponding voxels to a μ value approximate for 511-keV photons.

As an alternative to measured attenuation correction methods, calculated attenuation methods have been developed, which assume a regular geometric body outline and constant density. While these methods may be applicable for brain PET studies, they introduce significant artifacts, when applied to whole-body PET imaging studies.

Normalization

The thousands of detectors in a PET scanner do not necessarily respond uniformly to a given number of incident photons, either because of the relative efficiencies of the individual detectors, or because of the geometric arrangement of these detectors. As a result, there are slight variations in the coincidence detection efficiency or the sensitivity between different LORs in the system, for the same activity. Therefore, the entire projection data needs to be corrected (or normalized) for the differences in the detectors, response. This normalization corrects each individual LOR with a multiplication factor that compensates for these nonuniformities.

The direct method of determining the normalization correction factors is based on a direct measurement, in which a low-activity source of a positron emitter (such as ^{68}Ge) is used to acquire a scan (similar to a blank scan) in the 2D mode. Alternatively, a uniform cylinder of a positron-emitting radionuclide can be scanned and the data, thus, acquired, analytically corrected for attenuation. It is important to acquire enough counts per LOR to provide a good estimate of the efficiencies with minimum statistical noise.

For example, in order to achieve 1% accuracy in normalization for 10^6 LORs, it is necessary to acquire 10^{10} counts. If the radioactive source generates 25,000 cps, it would take 111.2 h (4.63 days) to acquire a normalization scan. For a 3D PET acquisition, the requirements for normalization are much more complicated.

An alternative method of generating normalization correction factors uses a combination of measurement and mathematical techniques. With current PET scanners, normalization scans are usually performed once a month, or every alternate month.

6.3.2.5 PET Image Reconstruction

The raw projection data of a PET emission scan only defines the location of the positron-emitting atom to within a line across the object. PET scanners allow the data to be collected from many different angles around the object. The main goal of the image reconstruction process is to provide quantitatively accurate cross-sectional images of the radiotracer distribution, in vivo, with the highest signal-to-noise ratio, and spatial resolution, using the emission scan data, and the mathematical algorithms of the CT. Basically, the reconstruction algorithms used in PET are classified into two different approaches: image reconstruction by filtered backprojection (FBP) and iterative reconstruction.

FBP involves two principal steps: filtering the projection data and then backprojecting them to create the reconstructed image. A mathematical tool, known as *Fourier transform*, is used in the FBP method to express a function $f(x)$ in terms of its spatial frequencies, rather than in terms of its magnitude as a function of its position (providing a mathematical description of these methods is beyond the scope of this chapter). One of the major limitations of the standard FBP method, used in tomography, is statistical noise. To control the noise and preserve the spatial resolution, an appropriate postreconstruction smoothing filter (such as Ramp, Shepp-Logan, Hann, Butterworth) needs to be applied.

Iterative reconstruction methods are computationally more intense than FBP and especially useful in reconstructing images with relatively poor counts. This method basically involves making an initial guess or estimates of the image distribution $a^*(x, y)$, comparing the forward projection sinogram of these estimates to the measured projection data sonogram, and, on the basis of the difference between these sinograms, revising the estimates. The process or the iterations continue until there is a convergence between the estimated and the measured sinogram. The iterative reconstruction algorithms allow for the incorporation of realistic modeling of the data acquisition process (including effects of attenuation and scatter) and modeling of statistical noise. The maximum-likelihood expectation maximization (ML-EM) algorithm is the most extensively studied iterative algorithm that seeks to maximize the Poisson likelihood target function. When the projection data are organized into *ordered subsets* (OS), the OSEM algorithm is used to accelerate the iterative computational process. Currently, OSEM is the most widely used iterative reconstruction algorithm used in 2D PET. Especially in the reconstruction of lower-count whole-body imaging studies, OSEM is preferable to the standard FBP.

As discussed earlier, 3D PET acquisitions increase scanner sensitivity, significantly. As a result, the 3D brain PET image reconstruction may be quite satisfactory with FBP methods. A technique known as *Fourier rebinning* (FORE) algorithm has been developed, which is appropriate for large 3D data sets, such as dynamic PET studies involving many frames. The gold standard for the analytic 3D image reconstruction, however, is the *3D reprojection* algorithm (3DRP), which is based on the FBP method. Whole-body 3D PET imaging with ^{11}C, ^{64}Cu, and ^{124}I radionuclides may be optimal to reconstruct on the basis of iterative methods although, the computational complexity increases, dramatically. The row-action maximization-likelihood (RAMLA) algorithm, related to the OSEM algorithm, has been developed for direct reconstruction of 3D PET images. With this method, the reconstruction times are fairly long by clinical standards, but it does provide reliable results.

6.3.2.6 PET Scanner Performance

Since the commercial PET scanners may have significant variations in the overall design of the scanner, certain parameters that determine the performance of the scanner must be determined using standard testing procedures. The National Electrical Manufacturers Association (NEMA) performance protocols describe a series of explicitly defined testing methods to evaluate PET and SPECT scanner performance. In order to illustrate the differences in scanner performance of commercial PET scanners, three scanners are compared in Table 6.5 (Humm et al 2003).

The spatial resolution (SR) of a system is a parameter that indicates the system's ability to distinguish between two points of radioactivity in an image and is measured in the transverse slice in two directions, radial and tangential, and in the axial direction. Generally, SR is measured at two axial positions: at the center of the axial FOV and a position one-fourth of the axial FOV from the center. SR is usually expressed as the FWHM and is usually specified separately in transaxial and axial directions.

Table 6.5 Comparison of PET scanners and scanner performance

Performance characteristic	CTI ECAT Exact (922)	HR^+	GE discovery LS PET/CT
Crystal	BGO	BGO	BGO
Patient Port (cm)	56.2	56.2	59
Total no. of blocks	144	288	168
No. of crystal detectors/block	8 × 8	8 × 8	6 × 6
Crystal size, transaxial, (mm)	6.39	4.39	4.0
Axial	6.39	4.05	8.0
Radial	20	30.0	30.0
Transaxial FOW (cm)	58.5	58.5	55
Axial FOW	16.2	15.5	15.2
Slice thickness (mm)	3.375	2.46	4.25
No. of slices	47	63	35
Sensitivity 2D trues, NEMA 94 phantom (kcps $\mu Ci^{-1}cc^{-1}$)	180	200	146
Sensitivity 2D trues + Scatter	214	244	159
Sensitivity 3D trues	780	900	838
Sensitivity 3D trues + scatter	1,218	1,406	1,297
2D axial resolution (mm)			
FWHM at 0 cm	4.5	4.2	4.0
FWHM at 10 cm	5.9	5.0	5.4
FWHM at 20 cm	N/A	6.8	6.6
3D axial resolution (mm)			
FWHM at 0 cm	4.6	3.5	6.0
FWHM at 10 cm	6.5	5.3	6.3
FWHM at 20 cm	N/A	7.8	6.6
2D transaxial resolution (mm)			
FWHM at 0 cm	6.0	4.6	4.8
FWHM at 10 cm	6.7	5.4	5.4
FWHM at 20 cm	N/A	7.9	6.2
3D transaxial resolution (mm)			
FWHM at 0 cm	6.0	4.6	4.8
FWHM at 10 cm	6.7	5.4	5.4
FWHM at 20 cm	N/A	7.8	6.2

Table modified from Humm et al. 2003

Energy resolution is the precision with which the PET scanner can measure the energy of incident photons (511 keV). It may be defined on the basis of either *single events* or *coincidence events* determined in air or in a scattering medium.

Count rate (counts per second, cps) performance refers to the finite time the system takes to process the detected photons. Count rate curves, as a function of increasing amounts of activity concentration (kBq cc^{-1}), can be generated for true (unscattered plus scattered) coincidences, as well as random and multiple coincidences. For most scanners, the true coincidence count rate is linear for activity (for ^{18}F) concentrations of <100 kBq cc^{-1}).

The sensitivity performance parameter of a scanner represents its ability to detect annihilation radiation, and the system sensitivity is considered the most important parameter since it determines the image quality per unit scan time or, alternatively, the time required to perform a whole-body scan (Humm et al. 2003). The absolute sensitivity of a scanner is expressed as the rate of detected coincidence events in counts per second (cps) for a given source strength. For a clinical scanner, the sensitivity depends principally on three main factors: the detector material, the axial field of view of the camera, and the acquisition mode (2D or 3D). With 3D, there is a marked increase in scatter and random events. The scatter fraction, defined as the

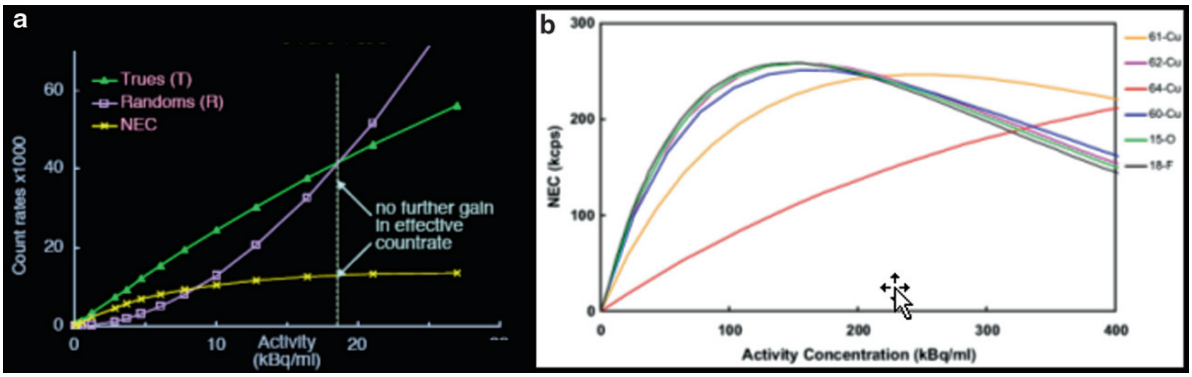

Fig. 6.9 Count rate with a PET scanner as a function of positron radionuclide concentration (**a**). Specifically, changes in NEC (**b**)

ratio of scattered events to total events, is independent of the activity within the patient, but is dependent on the patient's girth.

In order to provide a physical measure with which to assess PET camera performance, the concept of noise-equivalent count rate (NEC) was introduced. The NEC is defined as

$$\mathrm{NEC} = T^2 / (T + R + 2S)$$

where T is the true coincidence rate, R is the random coincidence, rate, and S is the scatter coincidence rate. T, R, and NEC as a function of activity concentration and variations in NEC as a function of activity concentrations for different PET radionuclides are shown in Fig. 6.9. It is important to recognize that for a positron emitter such as ^{64}Cu with <20% positron emission, *NEC* reaches the maximum value at 4–5 times the activity concentration generally needed for ^{18}F or ^{68}Ga.

6.3.3 Small-Animal Imaging Systems

Clinical imaging systems have relatively coarse spatial resolution that is insufficient for imaging structures in small animals, which requires high spatial resolution (on the order of 1–2 mm or better). To achieve this, scanners must use higher resolution detectors and achieve finer spatial sampling (e.g., using smaller detector elements) while maintaining as high a sensitivity as possible (Rowland and Cherry 2008). In the late 1990s, several groups began making significant progress in the development of high-resolution small-animal PET and SPECT scanners for the study of molecular imaging techniques in several rodent disease models (Chatziioannou 2002; Cherry 2004; Meikle et al 2005; Beekman et al 2005; Rowland and Cherry 2008). For both clinical and animal scanners, for a given size of the detector and field of view (FOV), there is a tradeoff between the resolution and the sensitivity, as shown in Table 6.6. For example, microPET scanners typically have at least 10 times greater sensitivity, than the microSPECT scanners. Some of the commercial animal scanners are listed in Table 6.7.

The first animal PET tomographs designed for imaging nonhuman subjects were the SHR-2000 developed by Hamamatsu (Japan) and the ECAT-713 developed by CTI PET Systems Inc. (Knoxville, TN). The first PET system developed specifically for rodent imaging was the RATPET scanner developed by Hammersmith Hospital in collaboration with CTI PET Systems Inc. The measured spatial resolution of this scanner was found to be 2.4 mm transaxially by 4.6 mm axially, giving a volumetric resolution of 0.026 cc. The 3D data acquisition of that system and the high detector efficiency provided a relatively high absolute sensitivity of 4.3%. Based on the UCLA MicroPET system, Concorde

Table 6.6 General scanncer performance characteristics compared between clinical and preclinical cameras.

	Clinical PET	Preclinical PET	Clinical SPECT	Preclinical SPECT
Sensitivity (%)	1–3	~2–4	0.01–0.03	~0.3
Resolution (mm)	~5	1–2	~10	0.5–2
FOV (cm)	~50	~7	~50	~8

Adapted from Jansen and Vanderhevden (2007)

Table 6.7 MicroPET and MicroSPECT Commercial Scanners

Company	MicroPET	MicroSPECT/CT
GE Healthcare	**Explore Vista PET** PET is based on LSO and LYSO coupled to APD detectors Options of 3 different axial fields of view, 3.75, 7.5, and 11.25cm **Triumph**, PET/SPECT/CT Multi-modality system	**Explore speCZT** Detector: pixilated Full Ring CZT with 8 slit collimator Resolution: 0.5 – 1.8 mm Axial FOV: 34 mm Transaxial FOV: 37 mm
Siemens	**Inveon MicroPET** based on LSO 1.59 × 1.59 × 10 cm pixel 12 cm Bore 12.7 cm Axial extent 64 Detector blocks **Inveon**, PET/SPECT/CT Multi-modality system	**Inveon MicroSPECT/CT** NaI(Tl) detectors with Two Multi-pinhole providing 0.5 – 1.0 mm resolution Four Single Pinhole providing 0.5 – 3.0 mm resolution
BioScan	**NanoPET/CT** Bore size: 15 cm Transaxial FOV: 94 – 125 mm Axial FOV up to 30 cm Detector: LYSO (39,780 crystals) Resolution: <1.2 mm	**NanoSPECT/CT** Multi-pinhole SPECT NaI(Tl) detectors Axial FOV up to 27 cm Resolution: up to 0.4 mm
MILabs		**U-SPECT/CT** Micro-pinhole technology NaI(Tl) detectors Resolution: 0.35 mm in 3D

Microsystems Inc. introduced the commercial microPET systems for primates (P4) and rodents (R4) based on a new generation of electronics designed to take full advantage of the fast decay time of the LSO detector. Since then, several other scintillator/PMT-based animal PET systems have been introduced.

In the last five years, there has been a significant improvement in the design of microSPECT systems for small-animal imaging studies. Because in microSPECT devices the required FOV is very small it is possible to achieve a much higher resolution than with clinical SPECT scanners. A number of commercial systems (Table 6.7) are now available with a spatial resolution <2 mm. Some of these devices even report submillimeter resolution for specific organs and tissues that may accumulate significant amounts of radioactivity. For most of the animal SPECT scanners, the detection efficiency for high-energy photons (<200 keV) is <0.1%. As a result, it is necessary to inject radiotracers at dose levels that are hundreds of times more than the clinical doses. Many of these devices are based on a wide variety of detection instrumentation, including conventional scintillation cameras, pixelated detectors with PSPMTs or APDs, and semiconductor gamma cameras.

References

Beekman FJ, van der Have F, Vastenhouw B, et al. (2005) U-SPECT-I: a novel system for submillimeter-resolution tomography with radiolabelled molecules in mice. J Nucl Med 46:1194–1200

Chatziioannou AF (2002) PET scanners dedicated to molecular imaging of small animal models. Mol Imaging Biol 4(1):47–63

Cherry SR (2004) In vivo molecular and genomic imaging: new challenges for imaging physics. Phys Med Biol 49:R13–R48

Darambara DG, Todd-Pokropek A (2002) Solid state detectors in nuclear medicine. Q J Nucl Med 46:3–7

Daube-Witherspoon ME, Karp JS, Casey ME, et al. (2002) PET performance measurements using the NEMA NU 2–2001 Standard. J Nucl Med 43:1398–1409

Humm JL, Rosenfeld A, Del Guerra A (2003) From PET detectors to PET scanners. Eur J Nucl Med Mol Imaging 30:1574–1597

Jansen FP, Vanderheyden J-L (2007) The future of SPECT in a time of PET. Nucl Med Biol 34:733–735

Jaszczak RJ (2006) The early years of single photon emission computed tomography (SPECT): an anthology of selected reminiscences. Phys Med Biol 51:R99–R115

Karakatsanis N, Sakellios N, Tsantilas NX, et al. (2006) Comparative evaluation of two commercial PET scanners, ECAT EXACT HR+ and Biograph 2, using GATE

Levin CS (2005) Primer on molecular imaging technology. Eur J Nucl Med Mol Imaging 32(suppl 2):S325–S345

Madsen MT (2007) Recent advances in SPECT imaging. J Nucl Med 48:661–673

Meikle SR, Kench P, Kassiou M, et al. (2005) Small animal SPECT and its place in the matrix of molecular imaging technologies Phys Med Biol 50:R45–R61

National Electrical Manufacturers Association (2001) NEMA Standards Publication NU 2–2001: Performance measurements of positron emission tomographs. NEMA, Rosslyn, VA

Nutt R (2002) The history of positron emission tomography. Mol Imag Biol 4(1):11–26

Pichler BJ, Wehrl HF, Judenhofer MS (2008) Latest advances in molecular imaging instrumentation. J Nucl Med 49:5s–23s

Rowland DJ, Cherry S (2008) Small-animal preclinical nuclear medicine instrumentation and methodology. Semin Nucl Med 38:209–222

Seo Y, Mari C, Hasegawa B (2008) Technological development and advances in single-photon emission computed tomography/computed tomography. Semin Nucl Med 38:177–198

Townsend DW (2008) Positron emission tomography/computed tomography. Semin Nucl Med 38:152–166

Zaidi H (2006) Recent developments and future trends in nuclear medicine instrumentation. Z Med Phys 16:5–17

Zanzonico P (2004) Positron emission tomography: a review of basic principles, scanner design and performance, and current systems. Semin Nucl Med 34(2):87–111